Davidson et al. Particle and Fibre Toxicology (2016) 13:23
DOI 10.1186/s12989-016-0134-8

Particle and Fibre Toxicology

RESEARCH Open Access

Direct stimulation of human fibroblasts by $nCeO_2$ *in vitro* is attenuated with an amorphous silica coating

Donna C. Davidson[1], Raymond Derk[1], Xiaoqing He[3], Todd A. Stueckle[1], Joel Cohen[2], Sandra V. Pirela[2], Philip Demokritou[2], Yon Rojanasakul[3] and Liying Wang[1*]

Abstract

Background: Nano-scaled cerium oxide ($nCeO_2$) is used in a variety of applications, including use as a fuel additive, catalyst, and polishing agent, yet potential adverse health effects associated with $nCeO_2$ exposure remain incompletely understood. Given the increasing utility and demand for engineered nanomaterials (ENMs) such as $nCeO_2$, "safety-by-design" approaches are currently being sought, meaning that the physicochemical properties (e.g., size and surface chemistry) of the ENMs are altered in an effort to maximize functionality while minimizing potential toxicity. *In vivo* studies have shown in a rat model that inhaled $nCeO_2$ deposited deep in the lung and induced fibrosis. However, little is known about how the physicochemical properties of $nCeO_2$, or the coating of the particles with a material such as amorphous silica ($aSiO_2$), may affect the bio-activity of these particles. Thus, we hypothesized that the physicochemical properties of $nCeO_2$ may explain its potential to induce fibrogenesis, and that a nano-thin $aSiO_2$ coating on $nCeO_2$ may counteract that effect.

Results: Primary normal human lung fibroblasts were treated at occupationally relevant doses with $nCeO_2$ that was either left uncoated or was coated with $aSiO_2$ ($amsCeO_2$). Subsequently, fibroblasts were analyzed for known hallmarks of fibrogenesis, including cell proliferation and collagen production, as well as the formation of fibroblastic nodules. The results of this study are consistent with this hypothesis, as we found that $nCeO_2$ directly induced significant production of collagen I and increased cell proliferation *in vitro*, while $amsCeO_2$ did not. Furthermore, treatment of fibroblasts with $nCeO_2$, but not $amsCeO_2$, significantly induced the formation of fibroblastic nodules, a clear indicator of fibrogenicity. Such *in vitro* data is consistent with recent *in vivo* observations using the same $nCeO_2$ nanoparticles and relevant doses. This effect appeared to be mediated through TGFβ signaling since chemical inhibition of the TGFβ receptor abolished these responses.

Conclusions: These results indicate that differences in the physicochemical properties of $nCeO_2$ may alter the fibrogenicity of this material, thus highlighting the potential benefits of "safety-by-design" strategies. In addition, this study provides an efficient *in vitro* method for testing the fibrogenicity of ENMs that strongly correlates with *in vivo* findings.

Keywords: Cerium oxide nanoparticles, Fibrosis, Engineered nanomaterials, Nanotoxicology, *in vitro* dosimetry

* Correspondence: LRojanasakul@cdc.gov
[1]National Institute for Occupational Safety and Health, Health Effects Laboratory Division, 1095 Willowdale Road, Morgantown, WV 26505, USA
Full list of author information is available at the end of the article

Background

Cerium, of the lanthanide metal group, is considered a rare earth metal. Rare earth metals have been reported to induce pneumoconiosis upon occupational exposure, with cerium found to persist in the alveoli and interstitial tissue for decades even after exposure has ceased [1]. Indeed, even the term "cerium pneumoconiosis" has been coined due to the increasing prevalence of such disorders [2, 3]. Use of cerium oxide nanoparticles ($nCeO_2$) has been steadily increasing across many industries, as it is an efficient polishing agent for glass, mirrors, and ophthalmic lenses. In addition, it has been utilized as a diesel fuel catalyst to aid in emission reduction, which subsequently leads to its release in the particulate phase of exhaust [4, 5]. Other uses of $nCeO_2$ in consumer goods are also in development, including use as an additive in cosmetics and sunscreens based on its UV absorption properties, and within the pharmaceutical industry. Thus, human exposure is inevitable in environmental, consumer, and occupational settings, with inhalation being the primary route of exposure.

Unfortunately, data is somewhat limited regarding human exposure concentrations to $nCeO_2$ in either occupational or environmental settings. However, several individual case studies of movie projectionists and photoengravers with regular exposure to $nCeO_2$ have noted the bio-persistence of these particles following occupational exposures, with associated lung disease [6, 7]. Considering the increased demand and use of this material, these reports highlight the need to fully characterize potential exposure-induced health effects associated with $nCeO_2$ use.

Consistent with this notion, several studies have been conducted in an effort to better understand $nCeO_2$-induced effects, with a focus on animal models of disease. These reports have noted the presence of $nCeO_2$-induced pulmonary inflammation, cardiovascular dysfunction, and fibrosis, as well as the bio-accumulation of $nCeO_2$, in agreement with the observed effects reported in human case studies [8–14]. Fibrosis is characterized by the excessive production of extracellular matrix (ECM) components around damaged lung tissue, which accumulate as the typical wound healing response mediated by fibroblasts aberrantly persists [15]. Under normal circumstances, following inflammation or injury, fibroblasts within the lung interstitium produce ECM proteins, such as collagen and fibronectin, in an effort to repair the damaged connective tissue. However, if left unchecked, fibrotic scarring can occur. Unfortunately, very few, if any, therapeutic strategies for the management of fibrosis currently exist, underlying the importance of devising strategies to limit the chances of developing fibrosis in occupational, consumer, and environmental settings.

Given the increasing utility and demand for engineered nanomaterials (ENMs) such as $nCeO_2$, "safety-by-design" approaches are currently being sought in an effort to maximize the functionality of ENMs while minimizing their potential toxicity and adverse health effects. One such strategy is the use of surface coatings, such as a nano-thin amorphous silica ($aSiO_2$) coating, that would provide a biologically inert shell while retaining the desired core material properties when possible [16]. Recent studies using $nCeO_2$ coated with $aSiO_2$ ($amsCeO_2$) have suggested that this approach may prove fruitful, as the coated version of $nCeO_2$ was able to substantially reduce $nCeO_2$-induced pulmonary inflammation, cytotoxicity, phospholipidosis, and fibrosis following acute exposure in rats [9, 17].

While these studies provide critical insight into the utility of this approach for designing safer ENMs, they were completed primarily using *in vivo* testing models. Given the high number of ENMs in development for countless uses, recently there has been a stronger initiative for more comprehensive *in vitro* models that would allow for more cost- and time-effective screening tools to identify potential toxicities and hazards associated with the use of these ENMs. Consistently, in the current report we sought to validate the reported *in vivo* findings that a nano-thin coating of $aSiO_2$ can limit the fibrogenicity of $nCeO_2$ [9, 17] using an *in vitro* model consisting of primary normal human lung fibroblast (NHLF) cell cultures. Employing the same $nCeO_2$ nanoparticles created using the Harvard Versatile Engineered Nanomaterial Generation System (VENGES), herein we report that $nCeO_2$ can directly stimulate NHLFs, inducing both proliferation and excessive collagen production, both of which are classic hallmarks of fibrogenesis. Furthermore, exposure to $nCeO_2$ significantly induced the formation of fibrotic nodules in cultured NHLFs. In clinical fibrosis, the presence and number of such fibrotic foci is one of the most reliable indicators of a poor prognosis [18–20]. As anticipated, the nano-thin $aSiO_2$ coating limited the fibrogenicity of $nCeO_2$, significantly decreasing the extent of $nCeO_2$-induced fibroblast proliferation, collagen production, and nodule formation, to levels resembling non-treated control cultures. Collectively these results further validate "safety-by-design" strategies for formulating ENMs and offer the details of a reliable *in vitro* model to analyze fibrogenicity that mimics results observed *in vivo*.

Results

Preparation and characterization of particle liquid suspensions for cellular studies

The nano-scaled cerium oxide ($nCeO_2$), amorphous silica-coated $nCeO_2$ ($amsCeO_2$), and the amorphous silica ($aSiO_2$) used in these studies were all generated using the Harvard VENGES method. The $aSiO_2$ was utilized in these studies as a control particle, since this is the particle with which the $nCeO_2$ was encapsulated to create the $amsCeO_2$ nanoparticle. In order to further validate our *in vitro* model as it relates to *in vivo* observations, we also included the use of an additional uncoated $nCeO_2$ that was not created using the

VENGES system, but rather, was purchased commercially from Sigma-Aldrich (denoted as Sigma in the figures) and was tested previously in a rat model in which it was found to induce fibrosis [10, 12]. Single-walled carbon nanotubes (SWCNTs) were also used as a positive control based on their previously reported fibrogenicity [21]. Table 1 summarizes particle characterization data in both powder form and in liquid suspension. Previously published transmission and scanning electron microscopic images of the VENGES $nCeO_2$ and $amsCeO_2$ samples collected *in situ* illustrate the fractal structure of the agglomerates formed by the flame synthesis method [17]. X-ray diffraction (XRD)-determined crystal size of uncoated $nCeO_2$ (17.3 nm) was slightly smaller than that of $amsCeO_2$ (21 nm). The specific surface area (SSA) of $nCeO_2$ was 61 m^2/g and the SSA of $amsCeO_2$ was 50 m^2/g, corresponding to an equivalent diameter of 12.8 nm and 19.2 nm, respectively. Differences between the $nCeO_2$ and $amsCeO_2$ Brunauer–Emmett–Teller (BET)-equivalent diameter are more pronounced than crystal sizes due to the $aSiO_2$ encapsulation, which is not accounted for when measuring the crystal size.

Both the intensity- and volume-weighted hydrodynamic diameter (d_H), as well as the zeta potential of $nCeO_2$, $amsCeO_2$, and $aSiO_2$ dispersed in sterilized deionized water (DI H_2O) and complete fibroblast growth media (FGM) are summarized in Table 2. The zeta-potentials measured for both $aSiO_2$ and $amsCeO_2$ dispersed in DI H_2O were strongly negative and significantly different from the strongly positive zeta potential measured for $nCeO_2$. All three particles exhibited similar zeta potential values around −12 mV when dispersed in FGM. Agglomerate diameters as measured via dynamic light scattering (DLS) were stable over the course of 24 h (data not shown). The intensity-weighted d_H for $nCeO_2$ was 229.7 nm, while that of $amsCeO_2$ was 288.3 nm when the particles were suspended in FGM. The polydispersity of both particles were below 0.5, which is indicative of distribution of monodispersed particles. Additionally, the volumetric centrifugation method (VCM)-measured effective density of $nCeO_2$ was 1.65 g/cm^3, whereas that of $amsCeO_2$ was 1.54 g/cm^3 when suspended in FGM.

Both the hydrodynamic diameter and the effective density of these formed agglomerates can greatly affect the fate and transport of the particles *in vitro*, in addition to defining settling rates, with significant implications for the dose of particles actually delivered to cells over the course of the *in vitro* toxicity assay. Thus, the delivered dose of nanoparticles may not always equal the administered dose [22–24]. In an effort to calculate the delivered-to-cell dose of $nCeO_2$, $amsCeO_2$, and $aSiO_2$, we employed the recently developed Harvard *in vitro* dosimetry method [22], which determines the fraction of the administered particles that is deposited onto the cells in the bottom of the well as a function of time (Table 3 and Fig. 1). As anticipated, the nanoparticles did not behave exactly the same in the FGM, with the $nCeO_2$ settling at a slower rate than both the $amsCeO_2$ and $aSiO_2$. While the $amsCeO_2$ and $aSiO_2$ achieved nearly 100 % deposition of the administered dose by approximately 24 h, roughly 70 % of the administered dose of $nCeO_2$ was delivered to the cells over the same time frame. $nCeO_2$ did not reach the same level of deposition as $amsCeO_2$ or $aSiO_2$ until at least 40 h post-treatment. Based on these results, the analyses reported herein were carried out 48 h post-exposure to the nanoparticles to allow for complete deposition of all particles.

Interestingly, the observed fibrogenic effects of $nCeO_2$ following a 24 h exposure did reveal a similar trend as the results presented herein that were obtained at the 48 h timepoint (data not shown). Although these results did not reach statistical significance at 24 h post-treatment, these findings highlight the increased fibrogenic potential of the $nCeO_2$ compared to the $amsCeO_2$, since there was roughly 30 % less deposition of the $nCeO_2$ at that time.

$nCeO_2$ induces proliferation and collagen I expression in fibroblasts

As previously mentioned, $nCeO_2$ is known to accumulate in the lungs in both humans and in animal models, and has been found in the pulmonary interstitium long after exposure has ceased [1, 6, 10]. This would suggest that $nCeO_2$ would directly contact resident lung cell types, including fibroblasts. In an effort to determine whether $nCeO_2$ directly stimulates fibroblasts, we measured two hallmarks of fibrosis, cell proliferation and collagen production. Primary

Table 1 Characterization of the engineered nanoparticles

Nanomaterial	Manufacturer	Manufacturing process	Theoretical $aSiO_2$ (wt%)	TCT (nm)	d_{XRD} (nm)	d_{BET} (nm)	SSA (m^2/g)
$nCeO_2$	Harvard University	VENGES FSP	0	0	17.3	12.8	61
$amsCeO_2$	Harvard University	VENGES FSP	20	3	21	19.2	50
$aSiO_2$	Harvard University	VENGES FSP	100	n/d	n/d	14	195
Sigma CeO_2	Sigma-Aldrich	n/d	0	n/d	n/d	20	n/d
SWCNT	CNI Houston	HipCo	0	n/d	n/d	n/d	400 – 1200

Abbreviations: *$nCeO_2$* uncoated $nCeO_2$, *$amsCeO_2$* amorphous SiO_2-coated $nCeO_2$, *$aSiO_2$* amorphous SiO_2, *n/d* measurement not determined or data not available, *VENGES FSP* versatile engineered nanomaterial generation system flame spray pyrolysis, *HipCo* high pressure CO disproportionation, *TCT* theoretical coating thickness, *d_{XRD}* x-ray diffraction calculated diameter, *d_{BET}* Brunauer–Emmett–Teller calculated primary particle diameter, *SSA* specific surface area

Table 2 Properties of ENM dispersions in DI H_2O and fibroblast growth medium

Nanomaterial	Media	Intensity-weighted d_H (nm)	PdI	Volume-weighted d_H (nm)	ζ (mV)	σ (mS/cm)	ρ_{agg} (g/cm^3)
$nCeO_2$	DI H_2O	262.5 ± 28.56	0.398 ± 0.03	n/d	47.3 ± 6.22	0.0051 ± 0.489	n/d
	FGM	229.7 ± 29.86	0.451 ± 0.11	187.79 ± 16.9	−12.6 ± 2.83	10.7 ± 0.306	1.65
$amsCeO_2$	DI H_2O	222.1 ± 8.86	0.249 ± 0.03	n/d	−50.3 ± 2.00	0.0031 ± 6.08e-5	n/d
	FGM	288.3 ± 5.43	0.354 ± 0.02	278.65 ± 11.8	−13.6 ± 0.92	8.00 ± 0.552	1.541
$aSiO_2$	DI H_2O	132.1 ± 4.45	0.190 ± 0.004	n/d	−36.4 ± 3.81	0.0026 ± 1.57e-4	n/d
	FGM	478.9 ± 35.31	0.437 ± 0.05	685.58 ± 263.9	−11.2 ± 2.18	13.0 ± 1.73	1.075

Abbreviations: *n/d* measurement not determined, d_H hydrodynamic diameter, *PdI* polydispersity index, *ζ* zeta potential, *σ* specific conductance, ρ_{agg} effective density. Values represent the mean (± SD) of a triplicate reading. Footnote: the average diameters obtained from DLS characterization are derived from the intensity-weighted distributions based on the intensity of light scattered by the particle

human fibroblasts were treated with a low dose, 0.006 μg/cm^2, as well as a high dose, 0.2 μg/cm^2, which correspond to the physiologically relevant doses that induced pulmonary fibrosis in a rat model [10, 12]. In these *in vivo* studies, the lowest dose of $nCeO_2$ tested was 0.15 mg/kg body weight. With an average weight of approximately 200 g per rat as noted in the report, this dose translates to approximately 30 μg per animal. Based on the rat lung surface area of 4000 cm^2, this corresponds to a dose of approximately 0.0075 μg/cm^2, which was sufficient to induce fibrosis at 84 days post-treatment. Using the same calculations, the 3.5 mg/kg dose corresponds to approximately 0.2 μg/cm^2, and this dose induced fibrosis 28 days post-treatment [10, 12].

Following treatment with both the low and high doses, cell proliferation was analyzed via nuclear stain and subsequent quantitation, which revealed that $nCeO_2$ significantly increased NHLF cell proliferation compared to non-treated cells (Fig. 2). In contrast, $amsCeO_2$ did not induce cell proliferation at either dose, similar to the $aSiO_2$ control, and treatment with the $amsCeO_2$ resulted in proliferation levels that were significantly lower than the $nCeO_2$ (Fig. 2). As mentioned, in order to further validate our *in vitro* model as it relates to *in vivo* observations, we also included the use of an additional uncoated $nCeO_2$, denoted as Sigma in the figures, which also induced cell proliferation at both doses tested, similar to the uncoated $nCeO_2$ obtained using the VENGES method.

Previous studies from our group have demonstrated that SWCNTs are directly fibrogenic to fibroblast cells, inducing cell proliferation as well as collagen production [21]. Thus, these particles were used as a positive control in the studies reported herein. As expected, SWCNTs also induced cell proliferation at levels similar to both uncoated $nCeO_2$ particles (Fig. 2). Similarly, the known fibrosis-inducing cytokine transforming growth factor beta (TGFβ) was used as a positive control and, as anticipated, invoked a significant level of proliferation in these cells.

As discussed, fibrosis is associated with the activation of fibroblast cells that stimulates the release and accumulation of extracellular matrix proteins such as collagen. Hence, collagen production was measured via Western blot analysis, as well as fluorescent microscopy, to determine whether $nCeO_2$ can induce the release of collagen directly from fibroblast cells. As demonstrated in Fig. 3, we observed a significant increase in collagen production in response to both uncoated $nCeO_2$ particles, as well as both positive controls, SWCNT and TGFβ, compared to non-treated cells. This effect was not observed in cells that had been treated with $amsCeO_2$. Furthermore, fibroblast cells treated with 0.2 μg/cm^2 of $nCeO_2$, as well as the Sigma CeO_2, SWCNTs, and TGFβ, demonstrated increased expression of alpha-smooth muscle actin (α-SMA), which indicates the activation and subsequent transformation of fibroblasts into myofibroblasts (Fig. 3c), the main source of collagen production during wound healing and fibrotic

Table 3 Relevant *in vitro* dose (RID) functions for $nCeO_2$, $amsCeO_2$, and $aSiO_2$ nanoparticles when dispersed in FGM

Nanomaterial	M	N	SA	RID_M	RID_N	RID_{SA}
$nCeO_2$ Low dose	0.01	2.08E-09	3.63E-16	0.01	1.08E-16	1.88E-23
$nCeO_2$ High dose	0.40	4.25E-01	4.53E-01	0.36	2.20E-08	2.35E-08
$amsCeO_2$ Low dose	0.01	6.82E-10	3.90E-17	0.01	5.88E-17	3.37E-24
$amsCeO_2$ High dose	0.40	3.10E-01	2.41E-01	0.39	2.68E-08	2.08E-08
$aSiO_2$ Low dose	0.01	6.56E-11	9.69E-05	0.01	3.11E-18	4.60E-12
$aSiO_2$ High dose	0.40	1.10E + 00	1.62E + 06	0.39	5.20E-08	7.68E-02

Delivered dose values based on delivered ENM mass (M), delivered particle number (N), and delivered surface area (SA) for either a high (0.57 μg/mL, equivalent to 0.2 μg/cm^2 for this study) or low (0.017 μg/mL, 0.006 μg/cm^2) dose

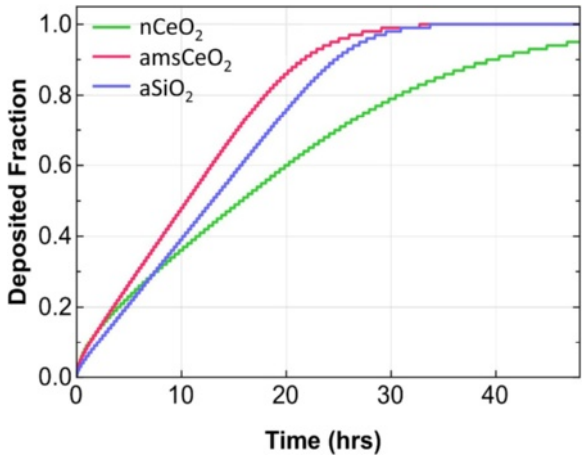

Fig. 1 Fraction of deposited $nCeO_2$, $amsCeO_2$, and $aSiO_2$ particles over a 48 h exposure, using fibroblasts cultured in 24-well tissue culture plates in fibroblast growth medium. The Harvard *in vitro* dosimetry method was used to determine the fraction of nanoparticle delivered to cells as a function of time. Uncoated $nCeO_2$ settled slower than both $amsCeO_2$ and $aSiO_2$, with all nanoparticles achieving approximately 90 % deposition by 40 h post-administration to cells

events. In contrast, the $amsCeO_2$, as well as the $aSiO_2$ alone, expressed α-SMA at levels similar to the non-treated cells. Taken together with the cell proliferation data, these results demonstrate that the $aSiO_2$ encapsulation of $nCeO_2$ is capable of attenuating the fibrogenic nature of the $nCeO_2$ as measured *in vitro*, in agreement with *in vivo* reports [9].

$nCeO_2$, but not $amsCeO_2$, induces the formation of fibroblastic nodules

We next utilized a fibroblastic nodule assay to further analyze the fibrogenicity of $nCeO_2$, as well as the effect that the encapsulation of this particle with $aSiO_2$ has on this process. A key pathological characteristic of fibrosis is the formation of fibrotic foci composed of fibroblasts, myofibroblasts, and accumulated collagen [18, 25, 26]. Consistently, formation of these foci *in vitro* is recognized as a useful method to assess the fibrogenic potential of nanomaterials. Primary human lung fibroblasts were plated on coverslips that had been coated with poly-L-lysine and subsequently treated with nanoparticles, as indicated, and nodule formation was assessed. As anticipated, we observed that both of the uncoated forms of $nCeO_2$ directly and significantly induced the formation of fibroblastic nodules in these cells in a dose dependent manner, as did both positive controls (Fig. 4). The $amsCeO_2$ did not induce extensive formation of fibroblastic foci, stimulating the formation of only a few foci per well, consistent with numbers observed in the non-treated cell cultures, and significantly less than $nCeO_2$. In addition, confocal microscopy z-stack analysis demonstrated that the fibrotic nodule clusters formed in response to $nCeO_2$ and TGFβ had an increased thickness as compared to the untreated monolayer of NHLFs, indicating the formation of multi-layer nodules (Fig. 4c).

Further analysis of the fibrotic nodules using enhanced darkfield imaging revealed that the $nCeO_2$ localizes at the site of nodule formation (Fig. 5). Consistently, SWCNTs also localized with the resulting fibrotic foci. Given that $nCeO_2$ has been shown to accumulate in the lungs following exposure [1, 6, 10, 27–29], this data would suggest that the formation of nodules may occur, at least in part, due to the accumulation of aggregated nanoparticles on the fibroblast cells that then respond to the foreign material in an aberrant manner.

The fibrogenic effect of $nCeO_2$ is mediated by TGFβ signaling

Finally, we sought to determine whether TGFβ signaling was the mechanism by which $nCeO_2$ was inducing stimulation of the fibroblast cells, since this mediator

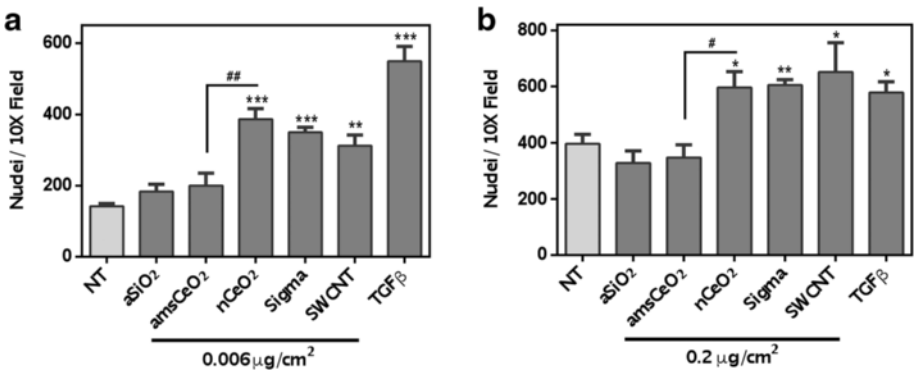

Fig. 2 $nCeO_2$ directly induces proliferation of NHLFs, while $amsCeO_2$ does not. Quantitation of DAPI stained nuclei of NHLFs that had been treated for 48 h was used to determine cell counts at the indicated doses and treatments. $nCeO_2$ induced a significant increase in cell proliferation at both 0.006 μg/cm^2 (**a**) and 0.2 μg/cm^2 (**b**) compared to non-treated cells as well as those treated with $amsCeO_2$. SWCNTs and TGFβ (1 ng/mL) were used as positive controls and also significantly increased proliferation of the fibroblast cells. Statistical significance is indicated as $*p < 0.05$, $**p < 0.01$, and $***p < 0.001$ compared to non-treated (NT) conditions and $\#p < 0.05$ and $\#\#p < 0.01$ for $nCeO_2$ compared to $amsCeO_2$

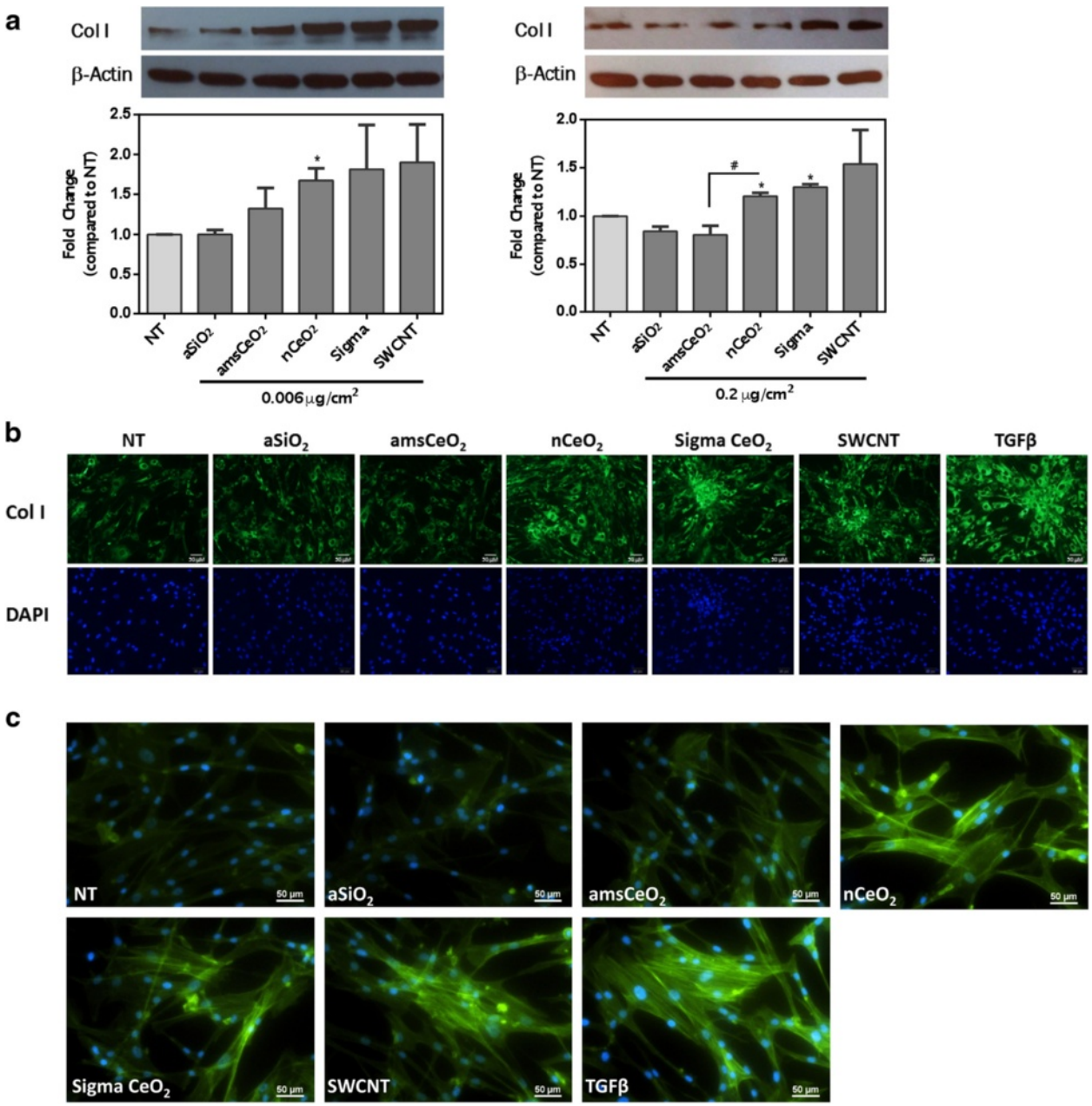

Fig. 3 $nCeO_2$ induces collagen I production from NHLFs, a hallmark of fibrosis, while $amsCeO_2$ does not. Primary human lung fibroblasts were treated with the indicated nanoparticle for 48 h. Western blot analysis with corresponding densitometry (**a**) and fluorescence microscopy (**b**) revealed a $nCeO_2$-induced increase in collagen I production, while the amorphous silica coating of $nCeO_2$ attenuated this observed effect on collagen production. SWCNTs and TGFβ (1 ng/mL) also significantly increased the expression of collagen I, as expected. (**c**) Alpha-smooth muscle actin staining of NHLFs that had been treated for 48 h with 0.2 μg/cm^2 of the indicated nanoparticle demonstrated that $nCeO_2$, as well as the Sigma CeO_2, SWCNTs, and TGFβ, increased expression of this myofibroblast marker. In contrast, the $amsCeO_2$, as well as the $aSiO_2$ control, expressed levels consistent with non-treated (NT) cells. Statistical significance is indicated as $^*p < 0.05$ compared to NT conditions and $\#p < 0.05$ for $nCeO_2$ compared to $amsCeO_2$

has been found to be upregulated following pulmonary instillation of $nCeO_2$ in rats [10], and is a known pro-fibrotic signal. As such, the TGFβ receptor inhibitor SB431542 was used, and fibroblast cells were incubated with this inhibitor for 3 h prior to the addition of nanoparticles. Following suppression of TGFβ signaling, $nCeO_2$-induced cell proliferation was diminished to levels resembling controls (Fig. 6a). Similarly, analysis of fibrotic nodule formation revealed that inhibition of TGFβ signaling attenuated $nCeO_2$-induced fibrogenicity

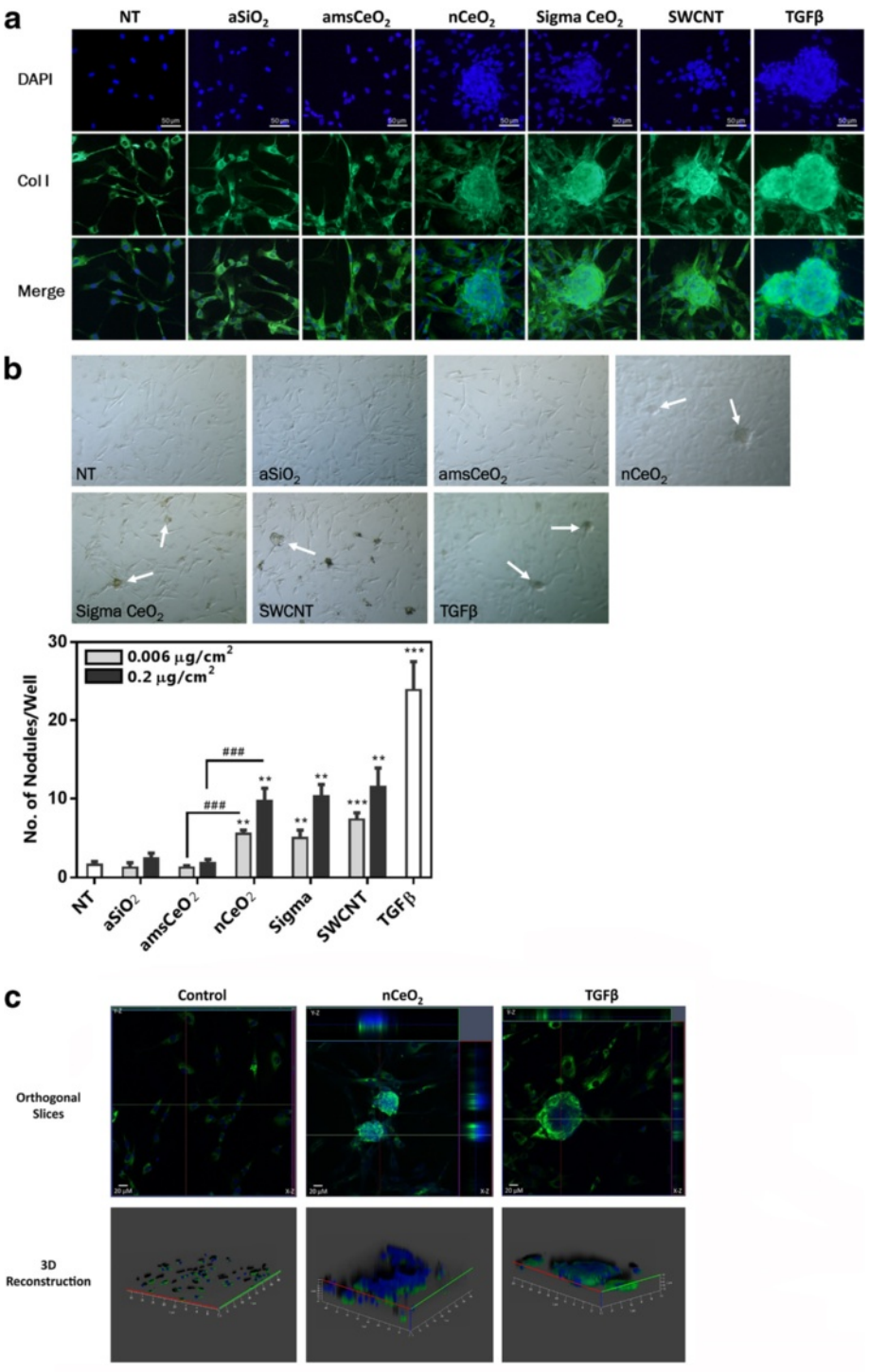

Fig. 4 (See legend on next page.)

(See figure on previous page.)
Fig. 4 $nCeO_2$, but not $amsCeO_2$, directly induces the formation of fibroblastic nodules in NHLFs in a dose dependent manner. Fibroblasts were plated on poly-L-lysine coated coverslips and treated with the indicated nanoparticle at 0.006 or 0.2 μg/cm^2 for 48 h. Cells were then stained for collagen I and DAPI and fibroblastic nodule formation was determined for each condition as the number of nodules formed per well. (**a**) Representative images of nodule formation in response to 0.2 μg/cm^2 of the indicated particles. Collagen I expression is shown in green and nuclear stain (DAPI) in blue. (**b**) Brightfield images of the fibroblastic nodules (arrows) were used to quantitate the number of nodules formed per well in response to each of the indicated nanoparticles. Statistical significance is indicated as $*p < 0.05$, $**p < 0.01$, and $***p < 0.001$ compared to non-treated (NT) conditions and $###p < 0.001$ for $nCeO_2$ compared to $amsCeO_2$. (**c**) Confocal microscopy Z-stack analysis with orthogonal views (upper panels) of the X-Z plane (right) and Y-Z plane (top). Three dimensional reconstruction was generated (bottom panels) based on the results of the Z-stack images and demonstrated increased thickness of fibrotic nodule clusters formed in response to $nCeO_2$ and TGFβ as compared to the untreated monolayer of NHLFs, indicating the mounding of the cells within the nodule

(Fig. 6b). Inhibition of TGFβ signaling also decreased collagen I production as induced by $nCeO_2$, demonstrated by decreased collagen I staining of NHLFs (Fig. 6c) and via western blot analysis (Fig. 6d). Collectively, these results indicate that $nCeO_2$ induces TGFβ signaling in fibroblast cells that ultimately leads to increased fibrogenicity.

Discussion

Use of $nCeO_2$ is quickly on the rise worldwide, with an increasing number of applications. Additionally, the increased use as a diesel fuel additive is leading to elevated levels of $nCeO_2$ released in diesel fuel exhaust, further increasing exposure to the general public [5]. Currently, reports of the implications of $nCeO_2$ treatment, both in cell culture models as well as animal models, tend to be conflicting in their determination of whether $nCeO_2$ is hazardous or safe. Indeed, some report the potential efficacy of this compound as a therapeutic agent based on its antioxidant and anti-inflammatory properties [30–32]. Still others, such as those discussed within this report, contend that $nCeO_2$ is a potential hazard due to its observed fibrogenicity. This discrepancy seems to be based primarily on the route of exposure, with inhalation being the most hazardous. These results, taken together with reports of $nCeO_2$-induced pulmonary disease and fibrosis following inhalation exposure [5, 6, 10, 12], raise public health concerns due to the fact that most current applications of $nCeO_2$ employed have the ability to generate respirable particles.

The potential health hazards caused by exposure to ENMs such as $nCeO_2$ has led to the development of alternative engineering methods to create safer materials while still maintaining the desirable characteristics of the material, commonly referred to as “safety-by-design” strategies. One such method employs a nano-thin layer of amorphous silica to “mask” the outside of the particle, since amorphous silica is considered to be relatively biologically inert [16, 33]. One main concern with these types of strategies is that the core material will no longer possess its desired properties once encapsulated. Indeed, in the case of CeO_2, the desirable catalytic properties may not be retained with an $aSiO_2$ coating; thus, depending on the application, this strategy may not always prove fruitful. However, when considering the observed results obtained in rat models, that $amsCeO_2$ causes less acute inflammation and pulmonary cell toxicity as compared to the uncoated $nCeO_2$, and minimizes markers of fibrosis such as the accumulation of surfactant in the air space and collagen production [9, 17], it seems that this strategy is worth pursuing when the application would tolerate such coatings. Consistent with this notion, nano-thin $aSiO_2$ coating

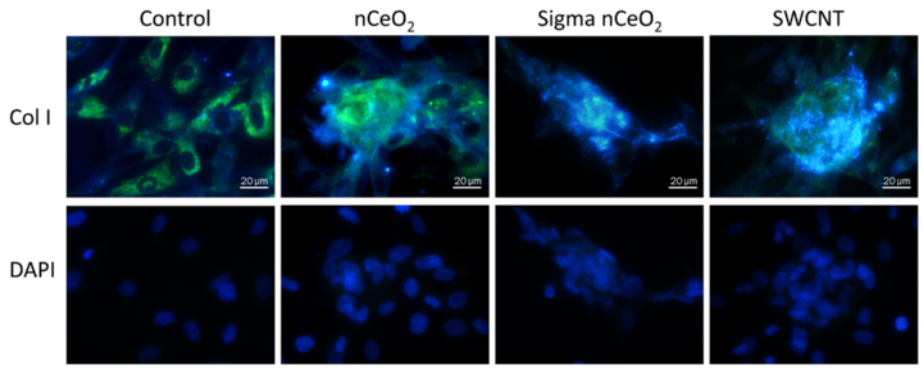

Fig. 5 $nCeO_2$ particles localize within fibroblastic nodules. NHLFs were treated with 0.2 μg/cm^2 of the indicated nanoparticle for 48 h. Following the treatments, cells were fixed, stained, and mounted onto glass, laser cut slides. Enhanced darkfield microscopy using the CytoViva illumination system revealed that the nanoparticles (bright spots) are localized on and around the fibroblastic nodules, suggesting that the accumulated particles may play a role in the initiation or formation of the nodules

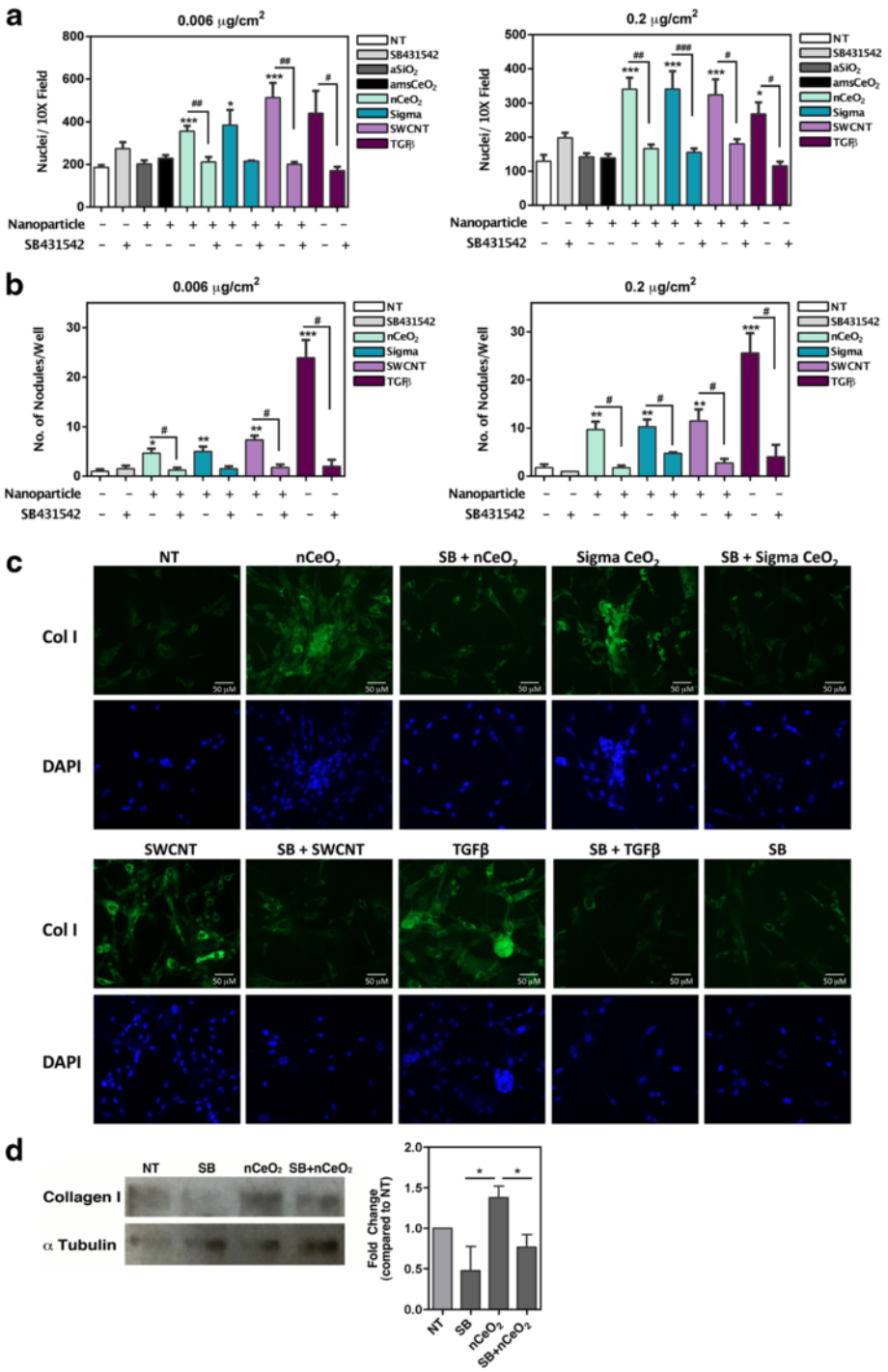

Fig. 6 $nCeO_2$ induced cell proliferation and fibroblastic nodule formation are attenuated with chemical inhibition of TGFβ receptor signaling. NHLFs were treated as indicated for 48 h. Cells receiving the TGFβ receptor inhibitor SB431542 (SB) were treated for 3 h with 1 μM of inhibitor prior to the addition of the nanoparticles. Chemical inhibition of the TGFβ receptor reversed the $nCeO_2$-induced increase in cell proliferation (**a**) and fibroblastic nodule formation (**b**) at both of the tested nanoparticle doses. (**c**) Collagen I staining demonstrated that inhibition of the TGFβ receptor decreased the $nCeO_2$-induced increase in collagen I production from NHLFs. (**d**) Western blot analysis and corresponding densitometry further confirmed that the SB inhibitor reversed the $nCeO_2$-induced increase in collagen I production. Statistical significance is indicated as $^{*}p < 0.05$, $^{**}p < 0.01$, and $^{***}p < 0.001$ compared to non-treated (NT) conditions or compared to other treatments as indicated in D; $\#p < 0.05$, $\#\#p < 0.01$, and $\#\#\#p < 0.001$ compared to the same treatment condition without inhibitor

also demonstrated a protective effect when used to encapsulate iron oxide, reducing both toxicity and genotoxic effects in two different cell types [34]. Collectively these reports, as well as the results demonstrated herein, validate this concept of "safety-by-design" for ENMs for further study and development.

As previously mentioned, current reports focused on $nCeO_2$ provide conflicting notions regarding the safety or potential toxicity of this nanoparticle. While some of these discrepancies can be attributed to the method of exposure, such as ingestion versus inhalation, others may be more attributable to differences in the toxicological experimental methods employed (e.g., dosing, timing, dispersion method, measured outcome). Unfortunately, there is limited data on actual human exposure concentrations to $nCeO_2$, and this makes predicting physiologically relevant doses somewhat difficult for experimental investigation. Likewise, nanoparticles are known to behave differently in various types of cell culture or dispersion media, often due to effects like the formation of protein coronas which can alter the bio-interactions of these particles once delivered to cells [17, 35, 36]. Several *in vitro* studies have examined the potential toxicity of $nCeO_2$, using numerous cell lines and endpoints, and most have concluded that $nCeO_2$ is relatively non-toxic and does not illicit a strong inflammatory response [17, 37–40]. On the contrary, when investigated *in vivo*, $nCeO_2$ has demonstrated both pro-inflammatory and pro-fibrogenic properties [8–10, 12, 14, 17, 41], which seems more consistent with the reported health effects observed in human case studies [6].

These apparent disparities between *in vitro* and *in vivo* results make evaluating the potential hazards of $nCeO_2$ difficult, and highlight the need for further development of more reliable and consistent *in vitro* models to study and predict the fibrogenicity potential of ENMs. This is especially important when considering the fact that animal studies can be time-consuming, costly, and limited in terms of high-throughput potential when screening a large number and variety of particles. Given the vast number of ENMs in use and in development, a number that continues to grow daily, this notion seems more critical than ever. Furthermore, *in vitro* cell models are useful in allowing more in depth analysis of the specific mechanisms employed by certain cell types as a result of exposure that cannot be assessed *in vivo* due to the complexity of the entire system. These mechanistic details can provide vital evidence that may be utilized for the purpose of developing therapeutic and diagnostic strategies or outcomes. For example, our model allowed us to utilize the TGFβ inhibitor SB431542 to investigate the extent to which TGFβ signaling plays a role in $nCeO_2$-induced fibrogenicity specifically in fibroblast cells, which we would not have been able to accomplish *in vivo* (Fig. 6). *In vivo* models will always remain a necessary approach to predict human response and potential disease outcomes, however, development of more novel, reliable *in vitro* methods would be extremely advantageous in helping to identify select agents that should be fully characterized using *in vivo* approaches.

In light of these concerns, we sought to develop a reliable *in vitro* model to examine the potential fibrogenicity of $nCeO_2$ using primary human fibroblasts. These cells present a desirable cell type for *in vitro* analysis of $nCeO_2$ since this particle is known to persist in the lung and has been found in the interstitium [1, 6, 10, 27–29]. Furthermore, *in vivo* models suggest that the primary negative outcome of exposure to $nCeO_2$ is fibrosis, which lends to the notion that fibroblast cells may be the main cell type involved in the biological response to $nCeO_2$. Thus, we directly treated primary human fibroblasts with $nCeO_2$ or $amsCeO_2$ to assess fibrogenicity. Our group has also previously employed this strategy to evaluate nanomaterials, specifically carbon nanotubes, and found that this model consistently correlated with *in vivo* outcomes [21, 42]. In the current report, we observed increased markers of fibrogenicity, cell proliferation, and collagen production (Figs. 2 and 3) when NHLFs were directly treated with $nCeO_2$ at physiologically relevant doses that match those reported *in vivo* [9, 10, 12]. $nCeO_2$ is relatively insoluble under typical cell culture conditions [43], indicating that the effects reported here are likely due to cellular interactions with particulate $nCeO_2$ rather than dissolved cerium. In addition, we saw a significant increase in the formation of fibrotic foci when the cells were treated with $nCeO_2$ (Fig. 4). These findings demonstrate that this *in vitro* model was able to accurately mimic results obtained using *in vivo* models [9, 10, 12, 17]. Similarly, our results accurately portrayed the observed *in vivo* effects of the nanothin amorphous silica coating of $nCeO_2$ when exposed to the NHLF cells, showing cell proliferation, collagen expression, and fibrotic nodule formation at levels consistent with non-treated and negative controls. These results also further validate the "safety-by-design" approach for further development of ENMs.

As mentioned, the higher dose of $nCeO_2$, 0.2 $\mu g/cm^2$, employed in our studies is equivalent, based on body weight and surface area of the rat lung, to the physiologically relevant dose that has been used in numerous *in vivo* models to initiate fibrosis. Indeed, using this dose we also observed the correlative fibrogenic potential of $nCeO_2$ in our *in vitro* model. Interestingly, the low dose of 0.006 $\mu g/cm^2$ used in these studies, which scarcely induces fibrosis *in vivo*, also induced a significant fibrogenic effect in our model. These results are noteworthy since they indicate that even very low levels of exposure may have the potential to initiate a fibrotic response. This is especially important in the case of nanomaterials when considering their bio-persistence. In addition, this

finding highlights the notion that reliable *in vitro* models may be useful in identifying potentially harmful doses of materials that would be relevant for follow up using *in vivo* models. Indeed, it plausible that interstitial fibroblasts would be exposed to lower doses of inhaled nanoparticles than other cell types of the lungs following exposure, due to factors such as clearance as well as translocation rate into the interstitium.

Conclusions

In summary, the results presented herein demonstrate that treatment of primary human lung fibroblasts *in vitro* is a useful approach for evaluating the potential fibrogenicity of nanomaterials that can efficiently represent results obtained *in vivo*. Furthermore, our results confirm those obtained using an *in vivo* rat model that a nano-thin coating of amorphous silica on the surface of $nCeO_2$ can successfully ameliorate the fibrogenicity of this nanomaterial. These results not only support the notion that "safety-by-design" strategies for developing ENMs are useful, but also demonstrate the utility of the current *in vitro* model for testing the fibrogenic potential of respirable nanoparticles.

Methods

Reagents and antibodies

Fibroblast basal medium, growth supplements, and NHLFs were purchased from Lonza (Walkersville, MD). Human-derived transforming growth factor beta (TGFβ), as well as the TGFβ receptor blocker SB431542, was obtained from R&D Systems, Inc. (Minneapolis, MN). Poly-L-lysine was purchased from Sigma-Aldrich (St. Louis, MO). The anti-Collagen I antibody was purchased from Fitzgerald (Acton, MA), while the alpha tubulin antibody was purchased from Santa Cruz Biotechnology, Inc. (Dallas, TX). Alexa-fluor 488-conjugated donkey anti-rabbit secondary antibody, alexa-fluor 488-conjugated alpha-smooth muscle actin (α-SMA) primary antibody, and the beta actin primary antibody were purchased from Abcam (Cambridge, MA). ProLong gold antifade with DAPI mountant was obtained from Molecular Probes (Thermo Fisher Scientific, Waltham, MA).

Particle generation and characterization

Nano-scaled CeO_2, $amsCeO_2$, and $aSiO_2$ particles were generated using the Harvard Versatile Engineered Nanomaterial Generation System (VENGES) and characterized as previously described [17]. Briefly, x-ray diffraction (XRD) patterns were obtained using a Scintag XDS2000 powder diffractometer [Cu Kα (λ = 0.154 nm), −40 kV, 40 mA, step-size = 0.02°]. The crystal size was determined by applying the Sherrer Shape Equation to the Gaussian fit of the major diffraction peak. The Brunauer–Emmett–Teller (BET) powder-specific surface area (SSA) of all samples was measured by nitrogen adsorption at 77 K (Micromeritics TriStar; Norcross, GA), after sample degassing for 1 h at 150 °C in nitrogen. BET equivalent primary particle size was calculated, under a spherical particle assumption, using $d_{BET} = 6000/(\rho \times SSA)$, where ρ is the material density.

Dry $nCeO_2$, $amsCeO_2$, and $aSiO_2$ particle dispersions in complete fibroblast growth medium (FGM) were prepared using a protocol developed by the authors [23], in which the particle-specific critical delivered sonication energy (DSE_{cr}), hydrodynamic diameter (d_H), formed agglomerate size distribution, polydispersity index (PdI), zeta potential (ζ), specific conductance (σ), pH, colloidal stability, and effective density of formed agglomerates are measured [44]. For treatment of cell cultures, particles were suspended in DI H_2O to acquire stock solutions of 0.1 mg/mL. Immediately prior to use, all particles were dispersed via sonication and subsequently diluted in FGM to the desired concentrations. Particles were then briefly vortexed and slowly added to the cultures.

Dosimetry

Subsequent to particle suspension, preparation, and characterization, the delivered-to-cell mass was calculated. Unlike soluble chemicals, colloidal suspensions of nanoparticles can have altered surface area, agglomerate formation, and settling rates depending on the suspension media, which may impact the bio-interactions of the particles when deposited onto cells in culture. Thus, dosimetric considerations must be taken into account. Therefore, the fraction of administered particle mass that is deposited on the cells as a function of *in vitro* exposure time (f_D) was calculated [22, 44] in order to accurately replicate the *in vivo* lung deposited doses of $nCeO_2$ [9, 10, 12]. The f_D as a function of *in vitro* exposure time was calculated using the hybrid Volumetric Centrifugation Method-*In Vivo* Sedimentation, Diffusion and Dosimetry (VCM-ISDD) methodology [22, 44, 45] developed by the authors. The mean media-formed volume-weighted agglomerate hydrodynamic diameter (d_H) and the VCM-measured effective density of formed agglomerates [44] were used as inputs to the VCM-ISDD fate and transport numerical model in order to estimate the f_D as a function of time.

Preparation of carbon nanotubes

Single-walled carbon nanotubes (SWCNT; Carbon Nanotechnologies, Inc., Houston, TX) were produced by the high pressure CO disproportionation (HipCo) technique, using CO in a continuous-flow gas phase as the carbon feedstock and Fe $(CO)_5$ as the iron-containing catalyst precursor. The SWCNTs were subsequently purified by acid treatment to remove metal contaminants. Nitric acid dissolution and inductively coupled plasma-atomic emission spectrometry (ICP-AES, NMAM #7300) were used to perform an elemental analysis of the supplied SWCNTs, and

indicated that they contained 99 % elemental carbon and 0.23 % iron. The specific surface area was measured at −196 °C by the nitrogen absorption-desorption technique (BET) using a SA3100 Surface Area and Pore Size Analyzer (Beckman Coulter, Fullerton, CA). The surface area of dry SWCNT was 400 – 1,000 m^2/g, and the length and width of individual (dry) SWCNT was 0.1 – 1 μm and 0.8 – 1.2 nm, respectively.

Dry SWCNTs were prepared for treatment as previously described and validated [46]. Briefly, particles were suspended in distilled water to acquire stock solutions of 0.1 mg/mL, which were supplemented subsequently with 150 μg/mL of a natural lung surfactant, Survanta (Abbott Laboratories, Columbus, OH) to aid in their dispersion. All particles were then dispersed using brief sonication and diluted in culture medium to the desired concentration.

Cell culture

NHLFs were obtained from Lonza (Walkersville, MD) and cultured in FGM, which is composed of Fibroblast Cell Basal Medium (FBM; Lonza) that contains all recommended growth supplements (FGM™-2 BulletKit™; Lonza). Cells were cultured and maintained at sub-confluent densities in a humidified incubator at 37 °C with 5 % CO_2. For each experiment, cells were seeded at density of 2.5 $\times 10^4$ cells per well in a 24-well plate the day before treatments were performed.

Immunofluorescence

Cells were seeded at a density of 2.5 × 10^4 cells per well onto glass coverslips that had been treated with poly-L-lysine (0.1 μg/mL), rinsed, and dried. Prior to their addition to cells, stock solutions of nanoparticles were sonicated and subsequently diluted in FGM to the desired concentration. Treated fibroblasts were incubated with nanoparticles for 48 h and were then fixed in 4 % paraformaldehyde and permeabilized using phosphate buffered saline containing 0.25 % Triton-X 100. Cells were then blocked with 2 % normal donkey serum and incubated with primary antibody raised against collagen I, followed by fluorescently conjugated secondary antibody. Cover glasses were then mounted on glass slides using ProLong Gold Antifade mountant with DAPI. Fluorescent and brightfield images were captured using a Zeiss Axiovert 100 TV inverted microscope (Carl Zeiss Microscopy, LLC, Thornwood, NY). For CytoViva images, coverslips were mounted onto laser-cut glass slides and images were captured using an Olympus BX-51 Microscope equipped with the CytoViva Advanced Dark field Illumination System (CytoViva, Auburn, AL) and a 100 W quartz-halogen light source.

Alternatively, cells stained for α-SMA were plated into chamber slides (Nalgene Nunc International, Naperville, IL) at a density of 1 $\times 10^4$ cells per well. Stock solutions of nanoparticles were sonicated and subsequently diluted in FGM to the desired concentration for cell treatment. Fibroblasts were incubated with nanoparticles for 48 h and cells were then fixed with 4 % paraformaldehyde in PBS solution on ice for 30 min and permeabilized with 2 % Triton-X 100 for 30 min at room temperature. After washing, cells were blocked with normal rabbit serum for 1 h and then incubated overnight at 4 °C with primary antibody raised against α-SMA that was conjugated with alexa-fluor 488. Cells were then washed and mounted with mounting solution containing DAPI (Vector Laboratories, Inc., Burlingame, CA). Images were taken using a Nikon Ti Eclipse fluorescent microscope.

Cell proliferation determination

Fibroblast cells were prepared, treated, and imaged as described for immunofluorescence. Resultant images were then analyzed for total cell numbers via Image J software (Bethesda, MD) by counting the total number of DAPI stained nuclei per 10X field. Four fields were captured per coverslip in duplicate for each of three independent replicates.

Immunoblot analysis and collagen I quantification

Following treatment, whole cell lysates were collected using cell extraction buffer (Life Technologies, Thermo Fisher Scientific, Waltham, MA) supplemented with 0.1 mM PMSF and a mixture of protease and phosphatase inhibitors. Cellular debris was removed by high-speed centrifugation and protein concentrations were then determined in each sample using the Pierce BCA Protein Assay (Life Technologies, Thermo Fisher Scientific, Waltham, MA). Samples (25 μg protein/lane) were separated on sodium dodecyl sulfate (SDS)-polyacrylamide gels and electrophoretically transferred to nitrocellulose membranes. The membranes were then analyzed with collagen I, beta actin, or alpha tubulin primary antibodies, and bound antibodies were detected using HRP-conjugated secondary antibodies. Densitometry was performed on the resulting bands using Image J software (NIH, Bethesda, MD) to quantitate the protein concentration in each sample.

Fibroblastic nodule assay

NHLFs were seeded onto glass coverslips that had been treated with poly-L-lysine (0.1 μg/mL) at a density of 2.5 $\times 10^4$ cells per well in a 24 well plate, and allowed to adhere overnight. Prior to their addition to cells, nanoparticles were sonicated using a cup sonicator and were diluted in FGM to the desired concentration. For experiments employing the TGFβ inhibitor SB431542, cells were incubated with 1 μM of the inhibitor for 3 h prior to addition of the nanoparticles. Fibroblasts were then incubated with nanoparticles for 48 h and were

subsequently fixed in 4 % paraformaldehyde and permeabilized using phosphate buffered saline containing 0.25 % Triton-X 100. Cells were then blocked with 2 % normal donkey serum and incubated with primary antibody raised against collagen I, followed by fluorescently conjugated secondary antibody. Cover glasses were then slowly washed and subsequently mounted on glass slides using ProLong Gold Antifade mountant with DAPI. Fluorescent and brightfield Images were captured using a Zeiss Axiovert 100 TV inverted microscope (Carl Zeiss Microscopy, LLC, Thornwood, NY). Confocal microscopy z-stack images were obtained using a Zeiss LSM780 confocal microscope. For each culture, two cover slides were analyzed and counted for nodule formation and data was pooled from three independent replicates.

Statistical analysis

Data represents mean ± SEM from three or more independent replicates and samples were analyzed using a one-way ANOVA with Tukey's post-test for multiple comparisons to determine significance. Statistical significance is indicated in each figure as $^{*}p < 0.05$, $^{**}p < 0.01$, and $^{***}p < 0.001$. All statistical analyses were performed using GraphPad Prism Software (La Jolla, CA).

Competing interests

The authors declare that they have no competing financial interests in the work described herein. In addition, the findings and conclusions presented in this manuscript represent those of the authors and do not necessarily represent the views of the National Institute for Occupational Safety and Health. The use of brand name does not constitute product support.

Authors' contributions

DCD designed and conducted experiments, analyzed data, and wrote the manuscript. RD, SVP, and JC prepared and characterized nanoparticles, contributed to experimental design, and edited the manuscript. XH, TAS, YR, and PD contributed to experimental design and data analysis, and edited the manuscript. LW supervised the study, contributed to experimental design and data analysis, and edited the manuscript. All authors read and approved the final manuscript.

Acknowledgements

The authors would like to thank Mark Barger and Dr. Jane Ma for their kind assistance with the study. This work was supported by the National Institute for Occupational Safety and Health, Nanotechnology Research Center Fund, and the National Science Foundation grants number 1235806 and 1434503.

Disclaimer

The findings and conclusions in this report are those of the authors and do not necessarily represent the views of the National Institute for Occupational Safety and Health.
Use of brand name does not constitute product support.

Author details

[1]National Institute for Occupational Safety and Health, Health Effects Laboratory Division, 1095 Willowdale Road, Morgantown, WV 26505, USA. [2]Department of Environmental Health, Center for Nanotechnology and Nanotoxicology, Harvard T. H. Chan School of Public Health, Boston, MA, USA. [3]Department of Pharmaceutical Sciences and Mary Babb Randolph Cancer Center, West Virginia University, Morgantown, WV, USA.

Received: 8 December 2015 Accepted: 26 April 2016
Published online: 04 May 2016

References

1. Pairon JC, Roos F, Iwatsubo Y, Janson X, Billon-Galland MA, Bignon J, Brochard P. Lung retention of cerium in humans. Occup Environ Med. 1994;51:195–9.
2. McDonald JW, Ghio AJ, Sheehan CE, Bernhardt PF, Roggli VL. Rare earth (cerium oxide) pneumoconiosis: analytical scanning electron microscopy and literature review. Mod Pathol. 1995;8:859–65.
3. Sabbioni E, Pietra R, Gaglione P, Vocaturo G, Colombo F, Zanoni M, Rodi F. Long-term occupational risk of rare-earth pneumoconiosis. A case report as investigated by neutron activation analysis. Sci Total Environ. 1982;26:19–32.
4. Cassee FR, van Balen EC, Singh C, Green D, Muijser H, Weinstein J, Dreher K. Exposure, health and ecological effects review of engineered nanoscale cerium and cerium oxide associated with its use as a fuel additive. Crit Rev Toxicol. 2011;41:213–29.
5. Health Effects Institute (HEI). Evaluation of Human Health Risk from Cerium Added to Diesel Fuel. HEI Communications, Volume 9. Boston, MA: Health Effects Institute; 2001.
6. EPA. IRIS Toxicological Review of Cerium Oxide and Cerium Compounds. U.S. Washington, DC: Environmental Protection Agency; 2009. EPA/635/R-08/002F.
7. Porru S, Placidi D, Quarta C, Sabbioni E, Pietra R, Fortaner S. The potencial role of rare earths in the pathogenesis of interstitial lung disease: a case report of movie projectionist as investigated by neutron activation analysis. J Trace Elem Med Biol. 2001;14:232–6.
8. Aalapati S, Ganapathy S, Manapuram S, Anumolu G, Prakya BM. Toxicity and bio-accumulation of inhaled cerium oxide nanoparticles in CD1 mice. Nanotoxicology. 2014;8:786–98.
9. Ma J, Mercer RR, Barger M, Schwegler-Berry D, Cohen JM, Demokritou P, Castranova V. Effects of amorphous silica coating on cerium oxide nanoparticles induced pulmonary responses. Toxicol Appl Pharmacol. 2015;288:63–73.
10. Ma JY, Mercer RR, Barger M, Schwegler-Berry D, Scabilloni J, Ma JK, Castranova V. Induction of pulmonary fibrosis by cerium oxide nanoparticles. Toxicol Appl Pharmacol. 2012;262:255–64.
11. Ma JY, Young SH, Mercer RR, Barger M, Schwegler-Berry D, Ma JK, Castranova V. Interactive effects of cerium oxide and diesel exhaust nanoparticles on inducing pulmonary fibrosis. Toxicol Appl Pharmacol. 2014;278:135–47.
12. Ma JY, Zhao H, Mercer RR, Barger M, Rao M, Meighan T, Schwegler-Berry D, Castranova V, Ma JK. Cerium oxide nanoparticle-induced pulmonary inflammation and alveolar macrophage functional change in rats. Nanotoxicology. 2011;5:312–25.
13. Minarchick VC, Stapleton PA, Porter DW, Wolfarth MG, Ciftyurek E, Barger M, Sabolsky EM, Nurkiewicz TR. Pulmonary cerium dioxide nanoparticle exposure differentially impairs coronary and mesenteric arteriolar reactivity. Cardiovasc Toxicol. 2013;13:323–37.
14. Srinivas A, Rao PJ, Selvam G, Murthy PB, Reddy PN. Acute inhalation toxicity of cerium oxide nanoparticles in rats. Toxicol Lett. 2011;205:105–15.
15. Wynn TA, Ramalingam TR. Mechanisms of fibrosis: therapeutic translation for fibrotic disease. Nat Med. 2012;18:1028–40.
16. Gass S, Cohen JM, Pyrgiotakis G, Sotiriou GA, Pratsinis SE, Demokritou P. A safer formulation concept for flame-generated engineered nanomaterials. ACS Sustain Chem Eng. 2013;1:843–57.
17. Demokritou P, Gass S, Pyrgiotakis G, Cohen JM, Goldsmith W, McKinney W, Frazer D, Ma J, Schwegler-Berry D, Brain J, Castranova V. An in vivo and in vitro toxicological characterisation of realistic nanoscale CeO(2) inhalation exposures. Nanotoxicology. 2013;7:1338–50.
18. Liu G, Friggeri A, Yang Y, Milosevic J, Ding Q, Thannickal VJ, Kaminski N, Abraham E. miR-21 mediates fibrogenic activation of pulmonary fibroblasts and lung fibrosis. J Exp Med. 2010;207:1589–97.
19. Lomas NJ, Watts KL, Akram KM, Forsyth NR, Spiteri MA. Idiopathic pulmonary fibrosis: immunohistochemical analysis provides fresh insights into lung tissue remodelling with implications for novel prognostic markers. Int J Clin Exp Pathol. 2012;5:58–71.
20. Meuten T, Hickey A, Franklin K, Grossi B, Tobias J, Newman DR, Jennings SH, Correa M, Sannes PL. WNT7B in fibroblastic foci of idiopathic pulmonary fibrosis. Respir Res. 2012;13:62.
21. Wang L, Mercer RR, Rojanasakul Y, Qiu A, Lu Y, Scabilloni JF, Wu N, Castranova V. Direct fibrogenic effects of dispersed single-walled carbon nanotubes on human lung fibroblasts. J Toxicol Environ Health A. 2010;73:410–22.
22. Cohen JM, Teeguarden JG, Demokritou P. An integrated approach for the in vitro dosimetry of engineered nanomaterials. Part Fibre Toxicol. 2014;11:20.

23. Cohen J, Deloid G, Pyrgiotakis G, Demokritou P. Interactions of engineered nanomaterials in physiological media and implications for in vitro dosimetry. Nanotoxicology. 2013;7:417–31.
24. Cohen JM, DeLoid GM, Demokritou P. A critical review of in vitro dosimetry for engineered nanomaterials. Nanomedicine. 2015;10(19):3015–32.
25. Cha SI, Groshong SD, Frankel SK, Edelman BL, Cosgrove GP, Terry-Powers JL, Remigio LK, Curran-Everett D, Brown KK, Cool CD, Riches DW. Compartmentalized expression of c-FLIP in lung tissues of patients with idiopathic pulmonary fibrosis. Am J Respir Cell Mol Biol. 2010;42:140–8.
26. Luanpitpong S, Wang L, Manke A, Martin KH, Ammer AG, Castranova V, Yang Y, Rojansakul Y. Induction of stemlike cells with fibrogenic properties by carbon nanotubes and its role in fibrogenesis. Nano Lett. 2014;14:3110–6.
27. Konduru NV, Jimenez RJ, Swami A, Friend S, Castranova V, Demokritou P, Brain JD, Molina RM. Silica coating influences the corona and biokinetics of cerium oxide nanoparticles. Part Fibre Toxicol. 2015;12:31.
28. Molina RM, Konduru NV, Jimenez RJ, Pyrgiotakis G, Demokritou P, Wohlleben W, Brain JD. Bioavailability, distribution and clearance of tracheally instilled, gavaged or injected cerium dioxide nanoparticles and ionic cerium. Environ Sci Nano. 2014;1:561–73.
29. Yokel RA, Hussain S, Garantziotis S, Demokritou P, Castranova V, Cassee FR. The yin: an adverse health perspective of nanoceria: uptake, distribution, accumulation, and mechanisms of its toxicity. Environ Sci Nano. 2014;1:406–28.
30. Eitan E, Hutchison ER, Greig NH, Tweedie D, Celik H, Ghosh S, Fishbein KW, Spencer RG, Sasaki CY, Ghosh P, et al. Combination therapy with lenalidomide and nanoceria ameliorates CNS autoimmunity. Exp Neurol. 2015;273:151–60.
31. Hashem RM, Rashd LA, Hashem KS, Soliman HM. Cerium oxide nanoparticles alleviate oxidative stress and decreases Nrf-2/HO-1 in D-GALN/LPS induced hepatotoxicity. Biomed Pharmacother. 2015;73:80–6.
32. Manne ND, Arvapalli R, Nepal N, Thulluri S, Selvaraj V, Shokuhfar T, He K, Rice KM, Asano S, Maheshwari M, Blough ER. Therapeutic potential of cerium oxide nanoparticles for the treatment of peritonitis induced by polymicrobial insult in Sprague–Dawley rats. Crit Care Med. 2015;43(11):e477–89.
33. Warheit DB, McHugh TA, Hartsky MA. Differential pulmonary responses in rats inhaling crystalline, colloidal or amorphous silica dusts. Scand J Work Environ Health. 1995;21 Suppl 2:19–21.
34. Malvindi MA, De Matteis V, Galeone A, Brunetti V, Anyfantis GC, Athanassiou A, Cingolani R, Pompa PP. Toxicity assessment of silica coated iron oxide nanoparticles and biocompatibility improvement by surface engineering. PLoS One. 2014;9:e85835.
35. Lundqvist M, Stigler J, Elia G, Lynch I, Cedervall T, Dawson KA. Nanoparticle size and surface properties determine the protein corona with possible implications for biological impacts. Proc Natl Acad Sci U S A. 2008;105:14265–70.
36. Walkey CD, Chan WC. Understanding and controlling the interaction of nanomaterials with proteins in a physiological environment. Chem Soc Rev. 2012;41:2780–99.
37. Dunnick KM, Pillai R, Pisane KL, Stefaniak AB, Sabolsky EM, Leonard SS. The effect of cerium oxide nanoparticle valence state on reactive oxygen species and toxicity. Biol Trace Elem Res. 2015;166:96–107.
38. Fisichella M, Berenguer F, Steinmetz G, Auffan M, Rose J, Prat O. Toxicity evaluation of manufactured CeO2 nanoparticles before and after alteration: combined physicochemical and whole-genome expression analysis in Caco-2 cells. BMC Genomics. 2014;15:700.
39. George S, Xia T, Rallo R, Zhao Y, Ji Z, Lin S, Wang X, Zhang H, France B, Schoenfeld D, et al. Use of a high-throughput screening approach coupled with in vivo zebrafish embryo screening to develop hazard ranking for engineered nanomaterials. ACS Nano. 2011;5:1805–17.
40. Xia T, Kovochich M, Liong M, Madler L, Gilbert B, Shi H, Yeh JI, Zink JI, Nel AE. Comparison of the mechanism of toxicity of zinc oxide and cerium oxide nanoparticles based on dissolution and oxidative stress properties. ACS Nano. 2008;2:2121–34.
41. Gosens I, Mathijssen LE, Bokkers BG, Muijser H, Cassee FR. Comparative hazard identification of nano- and micro-sized cerium oxide particles based on 28-day inhalation studies in rats. Nanotoxicology. 2014;8:643–53.
42. Mishra A, Stueckle TA, Mercer RR, Derk R, Rojanasakul Y, Castranova V, Wang L. Identification of TGF-beta receptor-1 as a key regulator of carbon nanotube-induced fibrogenesis. Am J Physiol Lung Cell Mol Physiol. 2015;309:L821–33.
43. Zhang H, Ji Z, Xia T, Meng H, Low-Kam C, Liu R, Pokhrel S, Lin S, Wang X, Liao YP, et al. Use of metal oxide nanoparticle band gap to develop a predictive paradigm for oxidative stress and acute pulmonary inflammation. ACS Nano. 2012;6:4349–68.
44. DeLoid G, Cohen JM, Darrah T, Derk R, Rojanasakul L, Pyrgiotakis G, Wohlleben W, Demokritou P. Estimating the effective density of engineered nanomaterials for in vitro dosimetry. Nat Commun. 2014;5:3514.
45. Pal AK, Bello D, Cohen J, Demokritou P. Implications of in vitro dosimetry on toxicological ranking of low aspect ratio engineered nanomaterials. Nanotoxicology. 2015;9:871–85.
46. Wang L, Castranova V, Mishra A, Chen B, Mercer RR, Schwegler-Berry D, Rojanasakul Y. Dispersion of single-walled carbon nanotubes by a natural lung surfactant for pulmonary in vitro and in vivo toxicity studies. Part Fibre Toxicol. 2010;7:31.